ELSEVIER

PII: S0266-3538(97)00197-8

Composites Sci. Technol. **58** (1998) 907–914

Printed in Great Britain
0266-3538/98 $—see front matter

INVESTIGATION OF THE MICROMECHANICS OF THE MICROBOND TEST

R. J. Day* & J. V. Cauich Rodrigez

Manchester Materials Science Centre, Grosvenor Street, Manchester M1 7HS, UK

(Received 18 August 1997; revised 15 September 1997; accepted 7 October 1997)

Abstract

The microbond test is a method which is sometimes used for measuring interfacial shear strength. In the analysis of the data it is often assumed that the interfacial shear stress is constant and thus, by implication, that the strain in the fibre along the embedded fibre decreases linearly from the point of entry to the point of exit. In this paper the results of conventional microbond tests and simulated microbond tests performed under a Raman microscope on a Kevlar-49/epoxy system are reported. The conventionally performed tests show that the calculated interfacial shear strength for this system is approximately 16 MPa regardless of the position of the supporting knife edges. The strain distribution along the fibre during simulated microbond tests was studied as a function of knife edge position, interfacial area and level of load by means of Raman spectroscopy. It was found that the interfacial shear stress was not constant, as is frequently assumed, but was strongly dependent upon distance through the droplet, knife-edge position and applied load. At low loads the strain was a maximum at the point where the fibre entered the droplet and then dropped off sharply through the embedded length. This effect was enhanced when the knife-edge separation was reduced. The variation of the shape of the stress distribution was similar to that predicted by a linear finite element analysis. At higher load levels the onset of failure in the region closest to the point where the fibre entered the droplet could be observed. © *1998 Elsevier Science Ltd. All rights reserved*

Keywords: A. aramid fibre, B. interface, B. interfacial strength, C. FEA, D. Raman spectroscopy

1 INTRODUCTION

Fibre-reinforced composites can exhibit outstanding properties compared to their constituents. The fibre, matrix and interface are all important factors in the performance of composites. In particular the effective utilisation of the strength and stiffness of the fibres depends upon efficient transfer of load through the interface and, therefore, good interfacial bonding. Toughness, however, can be promoted by the use of a weaker interface, as is the case in many ceramic-matrix composites. Thus the measurement and control of bond strength between the fibres and matrix is important and has been the subject of much effort. The interfacial shear strength of composites can be measured by tests on single-fibre systems.[1–13] It is noticeable, however, that the various tests give different results even when used to characterise the same system.[14,15] Of the single-fibre methods the most commonly used has been the pull-out technique.[1–8] A limitation to this approach is that if the fibre embedded length is longer than the critical length then failure of the fibre will occur before pull out. The manufacture of samples with sufficiently short embedded length is difficult. A modified technique, the microbond test, has been proposed in order to surmount this problem.[12,13] The sample preparation for this test involves the application of a microdroplet of resin onto the fibre. The microdroplet is then restrained by knife edges whilst the fibre is pulled out. It is usual to assume that the shear stress is constant along the interface so that the interfacial shear strength is calculated from the debonding force divided by the interfacial area. This should lead to a linear relationship between debonding force and embedded length. This relationship is observed if the embedded length is small, but at higher embedded lengths the debonding force tends to a maximum. This indicates that the assumption cannot be correct. Indeed theoretical and finite-element studies show that the interfacial shear stress is not constant throughout the specimen.[16–19] It is clear that experimental measurements of the strain and interfacial stress distributions along the interface during the microbond test are required in order to put the theory and data reduction method on a firmer footing.

It has been found that the frequency of the bands in the Raman spectrum of many materials is sensitive to the stress in that material. There are a large number of reports which show that Raman spectroscopy can be used to measure strain and shear stress in fibres and

*To whom correspondence should be addressed.

composites.[20–34] Kevlar fibres have been the subject of a number of these studies as single fibres, in composites and during micromechanical tests.[18,24–34] There has been some confusion in the literature since some authors have not found changes in the Raman spectrum of Kevlar when the fibre was loaded.[35,36] These authors used high powered argon-ion lasers whereas those who found shifts used helium–neon lasers.[21,27,29–32] It is now clear that the 488 nm line of argon-ion lasers causes erratic Raman peak shifts and premature failure when used to excite Raman spectra from Kevlar fibres.[21] In this work Raman spectroscopy was used to obtain the strain distribution along a fibre within a droplet during simulated microbond tests using a helium neon laser and from these data the interfacial shear stress distributions were determined.

2 EXPERIMENTAL

Microbond tests were carried out using an Instron mechanical testing machine in order to provide a comparison between the Raman data and the conventional approach. The Kevlar fibres were mounted singly upon paper cards with windows cut in them using double-sided adhesive tape. The fibres were subsequently fastened with a slow setting, cold-curing epoxy adhesive. The fibre droplet specimens were prepared by depositing a small amount of epoxy resin onto a horizontally suspended Kevlar fibre. The epoxy resin used was Ciba-Geigy LY1927 and the hardener was HY1927. These were mixed in the recommended ratio of 100:36 parts by weight and cured at room temperature. The resin was placed on the fibre with a fine glass applicator under a magnifier. The embedded length and droplet diameter were measured for each sample under an optical microscope. Microbond tests were performed with the mechanical testing machine. The free end of the fibre was held in a standard fibre testing grip. The microdroplet was restrained by using two knife edges. The separation of these was controlled by means of a micrometer. A schematic drawing of the arrangement is shown in Fig. 1.

The Raman spectroscopic measurements were performed on a SPEX 1000 m single spectrometer coupled to a modified Olympus BH-2 optical microscope. Additional rejection of the laser line was provided by a holographic filter placed between the microscope and spectrometer. A Wright Instruments CCD camera was used as the detector. Spectra were excited with the 632·8 nm line of a 7 mW helium neon laser. The power at the sample was less than 1 mW. The beam was focused on the sample through the microscope using a ×20 objective lens with a numerical aperture of 0·4. The beam was polarised parallel to the fibre axis for all measurements and the exposure time was ten seconds. Prior to the simulated microbond experiments a number of calibration curves of strain versus Raman frequency were obtained. Single Kevlar fibres were fastened to a purpose built straining rig consisting of one fixed and one moveable block. The latter was displaced by a micrometer, thus giving a measurement of fibre strain. Spectra of the 1610 cm^{-1} band were taken at 0·1% increments in fibre strain. The gauge length of the samples was approximately 20 mm.

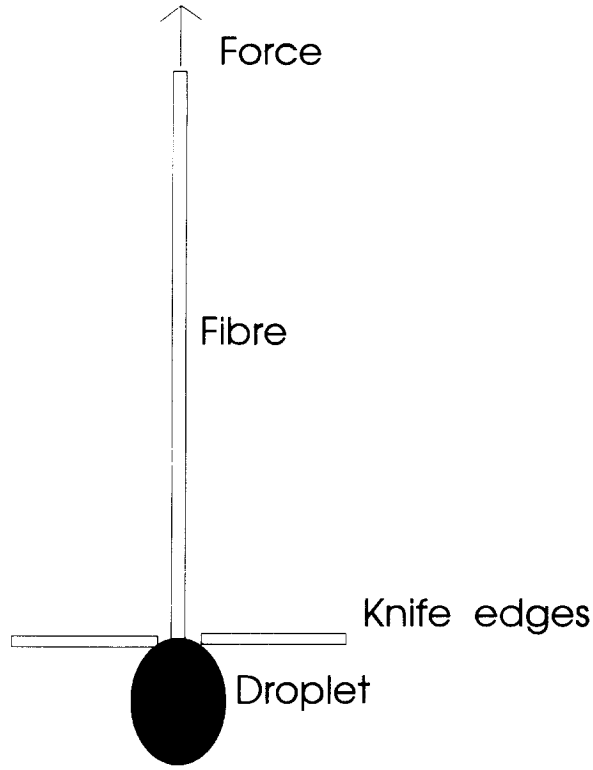

Fig. 1. Schematic diagram of the experimental arrangement used to obtain debonding force versus embedded area data.

The simulated microbond tests were carried out using a straining rig which was modified from the one used for the single-fibre calibration measurements. A schematic diagram of this rig is shown in Fig. 2. The stationary block was replaced by two adjustable knife edges which allowed the resin droplet to be restrained with different knife edge separations. For these experiments gaps of 20, 50 and 80 μm were used. The end of the fibre was fastened to the moveable block in a similar manner as in the single-fibre tests. The fibre was strained to a number of levels of strain and at each, spectra were taken from the embedded fibre. Spectra were taken at 10 μm intervals in the first 100 μm from the point where the loaded fibre entered the droplet, then at 30 μm intervals after that. Spectra were also taken from the area either side of the knife edges and also from the loaded fibre. Samples with droplets from 100 μm to 600 μm in length were used.

Finite-element simulation of the microbond test was used to observe the effect of the knife edge separation upon the form of the shear stress distribution along the interface. This was undertaken with the LUSAS finite-element system from FEA Ltd. A linear–elastic

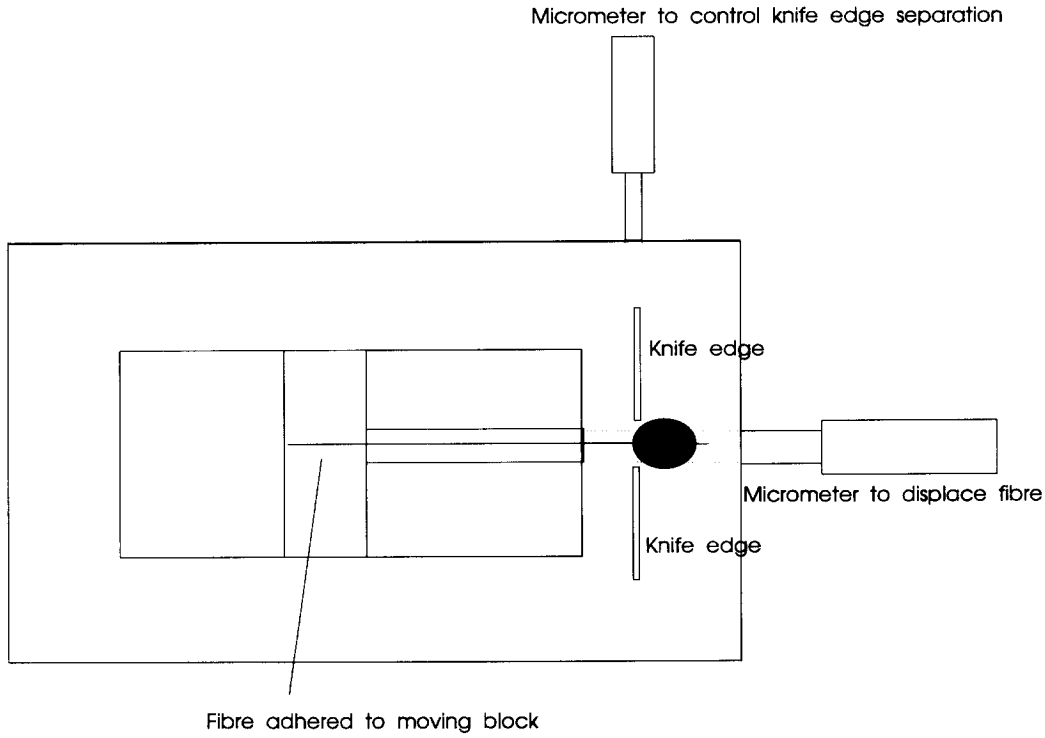

Fig. 2. Schematic diagram of the apparatus used to perform the simulated microbond tests.

axisymmetric model was used. The axial modulus of the fibre was assumed to be 121·5 GPa and the transverse modulus 2·49 GPa.[37] The shear modulus of the fibre was taken to be 1·69 GPa.[38] The resin Young's modulus was assumed to be 3 GPa.

3 RESULTS AND DISCUSSION

3.1 Conventional analysis

Conventional microbond tests were carried out in an Instron mechanical tester as described earlier. The droplets were supported by knife edges. One of these was moved by means of a micrometer so that the separation between them could be set. Experiments were carried out with knife-edge separations of 20, 50 and 80 μm. Figures 3–5 show plots of pull-out force against embedded area data obtained with these knife edge separations. According to Miller *et al.*[13] the shear stress can be assumed to be constant along the interface and thus the interfacial shear strength can be found from

$$\tau = \frac{F}{2\pi rl} \tag{1}$$

were F is the failure force, r is the radius of the fibre, l is the embedded length and hence 2πrl is the embedded area. Straight lines were fitted to the failure force against interfacial area data in Figs 3–5. Only the data at low embedded areas were used for this because as the embedded area increases the data tends towards a constant value of force. At this constant level of applied force it is quite possible that the fibre is failing rather than interfacial yielding or debonding occurring. The fits were forced to go through the origin since it is clear from Equation 1 that the force must be zero when the embedded area is zero. The straight line fits yield values of average interfacial shear strengths of 15·7, 15·8 and 15·5 ± 3·0 MPa for tests with the knife edge separations of 20, 50 and 80 μm, respectively. Thus the position of the knife edges appeared to have no effect upon the measured value of interfacial shear strength. This should be compared to the data obtained from simulated microbond tests using Raman spectroscopy, presented in the next part of the paper, which shows a

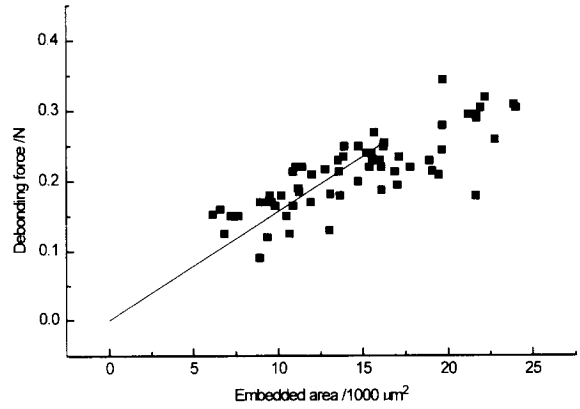

Fig. 3. Plot of debonding force vs embedded area measured for Kevlar-49 fibres in Ciba Geigy LY1927 resin with a knife edge separation of 20 μm.

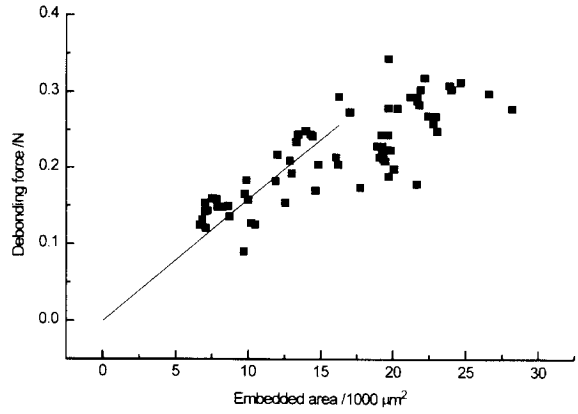

Fig. 4. Plot of debonding force vs embedded area measured for Kevlar-49 fibres in Ciba Geigy LY1927 resin with a knife edge separation of 50 μm.

significant variation in the interfacial shear stress distribution depending upon the position of the knife edges.

3.2 Raman investigations of microbond samples at low strain levels

In order to investigate in more detail the micromechanics of the microbond tests, Raman microscopy was used to measure the stress distribution along the interface. In order to use this approach it is necessary to calibrate the rate of shift of one of the Raman bands with strain for a single fibre. This was accomplished using a small straining rig as described earlier. Figure 6 shows a calibration plot for a single Kevlar fibre. The average slope measured was 4·85 cm^{-1} $\%^{-1}$ which is in good agreement with previously published values.[21,31]

Simulated microbond tests were performed in a rig similar to that used for calibrating the single fibres as described earlier. The simulated microbond tests were difficult in general to perform. Raman spectra were obtained from a number of specimens with different embedded lengths to investigate the effect of embedded length on the strain distribution along the interface and upon the interfacial shear stress distribution. The effect of knife edge separation upon these distributions was also investigated. The simulated microbond test samples all failed by debonding except in one case where the embedded length was 500 μm and the knife separation was 20 μm which failed by fibre fracture. Since only one sample failed this way this may have been a result of the high stress on the fibre at the point of entry caused by the support conditions or by rubbing of the fibre against the knife edge.

Figure 7 shows typical results from some simulated microbond tests. Three strain profiles are presented, each taken with knife edge separations of 20, 50 and 80 μm. The external fibre strain was between 0·6 and 0·9% for these data. Information with fibres at exactly the same strain was not obtained because of the difficulties in making the measurements. The droplets in each case were approximately 500 μm long. There is some scatter in the data, but it can be seen that the strain in the fibre is a maximum close to the point where the loaded fibre enters the droplet and the strain rapidly decreases along the length of the droplet. This is as might be expected from shear lag theory,[39,40] but is contrary to the assumption made in the simple analysis of the microbond test,[12,13] that the shear stress is constant. In order for the shear stress to be constant the decrease of strain with distance through the droplet should be linear, which is not the case as shown by Fig. 7.

The pull-out test was modelled by a number of workers. The general form of these models is very similar. Piggott[17] gives the strain along the fibre, ε_f, as

$$\varepsilon_f = \varepsilon_{app} \frac{\sinh[n(L_e - x)/r]}{\sinh(ns)} \tag{2}$$

where ε_{app} is the external strain on the fibre, r is the radius of the fibre, L_e is the embedded length, s is the aspect ratio of the fibre, i.e. L_e/r and n is given by the formula

$$n^2 = \frac{E_m}{E_f} \frac{1}{\ln(R/r)} \frac{1}{(1 + \nu_m)} \tag{3}$$

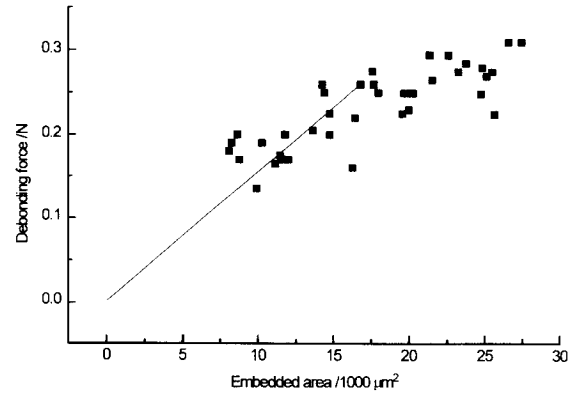

Fig. 5. Plot of debonding force vs embedded area measured for Kevlar-49 fibres in Ciba Geigy LY1927 resin with a knife edge separation of 80 μm.

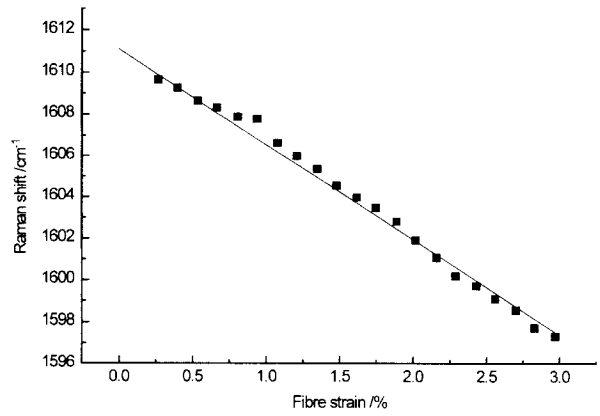

Fig. 6. Calibration of rate of change of position of the 1610 cm^{-1} band in Kevlar with strain.

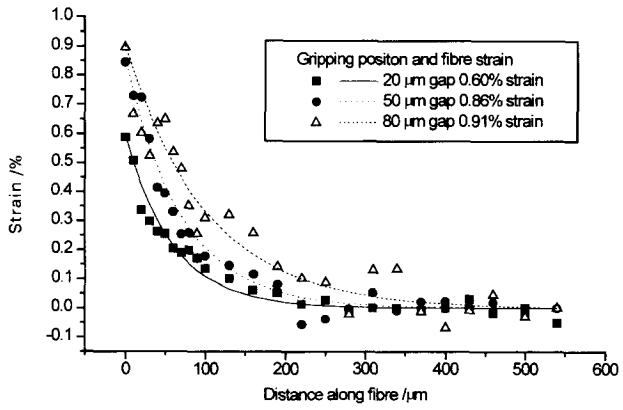

Fig. 7. Strain distribution in droplets of approximately 500 μm length at various knife edge separations.

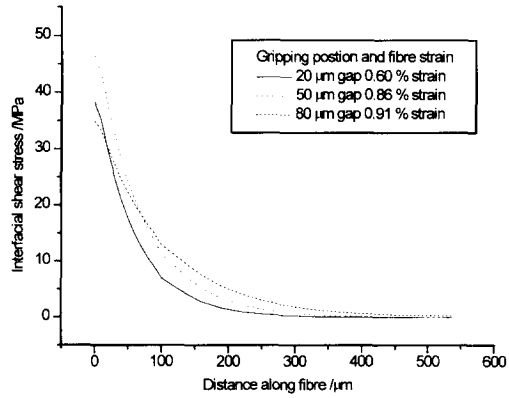

Fig. 8. Interfacial shear stress distribution in droplets of 500 μm length at various knife edge separations calculated from the data of Fig. 7.

where E_m is the Young's modulus of the matrix, E_f is the fibre Young's modulus, R is the radius of the block of resin surrounding the fibre, r is the radius of the fibre and ν_m is the Poisson's ratio of the matrix

In order to ascertain whether or not the theory predicts the form of the data, Equation 2 was plotted with the strain data obtained from a droplet of length 540 μm in Fig. 7. It can be seen in Fig. 7 that eqn (2) fits the data reasonably well. In order to plot these curves a value for n of 0·11 was used for the data gathered with knife edge separations of 20 and 50 μm and 0·07 for the data obtained with a knife edge separation of 80 μm. The difference in the value of n required to fit the data where the droplet was gripped further away from the fibre suggests that at this point the influence of the knife edges upon the strain and interfacial stress distributions is less marked. The significance in the different values of n required to fit the data is not high, however, and thus n should be regarded as little more than a fitting constant. Although the theory was developed for the pull-out rather than microbond test the geometry is similar and the fit to the experimental data can be seen from Fig. 7 to be good.

3.3 Geometrical effects

Closer inspection of Fig. 7 reveals that the slope of the curves for different gripping positions is not the same. The rate of decrease of fibre strain with distance into the droplet is lower for the droplet restrained with an 80 μm knife edge gap than for the ones where the knife edge separation was 20 or 50 μm. In order to fit the data, as noted earlier, a different value of n was required. This difference is, as stated previously, presumably owing to the influence of the stress concentration of the knife edge at the lower separations.

Perhaps clearer, is the data presented in Fig. 8 which shows the interfacial shear stress as a function of position through the droplet. This was calculated from the data of Fig. 7 using the expression[41]

$$\tau_x = \frac{E_f d}{4} \frac{\mathrm{d}e_f}{\mathrm{d}x} \qquad (4)$$

where τ_x is the interfacial shear stress, E_f is the fibre Young's modulus, d is the fibre diameter and $\mathrm{d}e_f/\mathrm{d}x$ is the slope of the strain against distance curve. These data show that the interfacial shear stress is high at the point of entry of the fibre into the droplet and then decreases rapidly with distance through the droplet.

Figure 8 shows that the interfacial shear stress at the point of fibre entry into the droplet increases as the knife edge supports are moved closer towards the fibre. There is thus an influence on the strain and stress distributions of the gripping position.

In order to verify the stress distributions obtained from the Raman spectroscopy experiments and to model the effect of knife edge position upon the strain distributions a simple, linear axisymmetric finite element analysis was performed. In this analysis the gripping position was moved around the droplet one node at a time from the fibre outwards. The mesh which was used is shown in Fig. 9. Figure 10 shows the strain distribution in the droplet as a function of the gripping position predicted by the finite element analysis. The external fibre strain used for these calculations was 1%. Comparison of this with Fig. 7 shows good agreement on the shape of the stress distribution, thus confirming the experimental measurements. It is clear from these measurements and calculations that the interfacial shear stress in the droplet will not be constant, as is usually assumed in the analysis of data from this test.

Figure 11 shows the effect of droplet length on the strain distribution in the embedded part of the fibre. In this figure the separation of the knife edges was

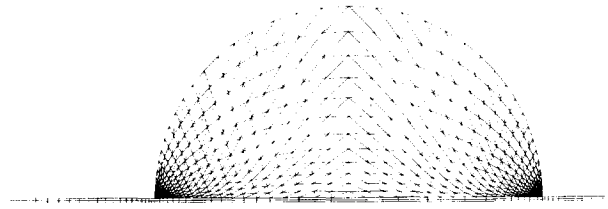

Fig. 9. Finite element mesh used in numerical modeling of the microbond test.

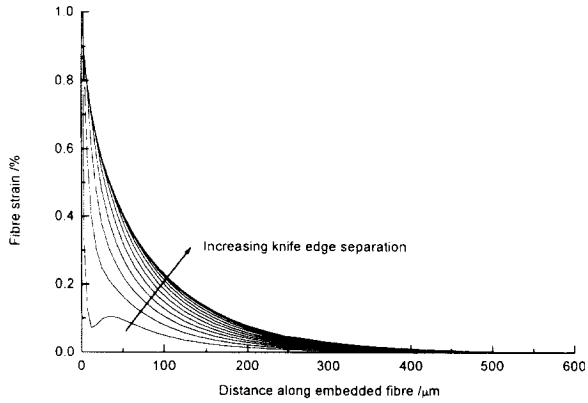

Fig. 10. Strain distribution along the interface in a droplet of length 540 μm calculated using a linear elastic finite element model. The curves were generated by moving the gripping position away from the fibre one node at a time and rerunning the analysis.

maintained at 80 μm. It can be seen from Fig. 11 that for the embedded lengths examined that the strain distributions are similar in nature to those observed in Fig. 7. The strain decreases throughout the droplet, but this decrease is not linear and, therefore, cannot give a constant shear interfacial shear stress. The form of this decrease is similar in each of these cases and not dissimilar to the form of the shear lag and finite element[17,19,30] predictions.

3.4 High-strain deformation

So far all of the strain and shear stress distributions presented and discussed have been recorded with the strain in the loaded part of the fibre being 1% or less. Thus the specimen is not close to failure and the matrix is still behaving elastically. The stress distributions close to failure might be expected to be different to these initial ones. This is true for this system and Fig. 12 shows the strain distribution in a 440 μm long droplet, with the knife edges 50 μm apart at different levels of applied stress. It can be seen from this figure that the strain distribution within the fibre at low strain levels is

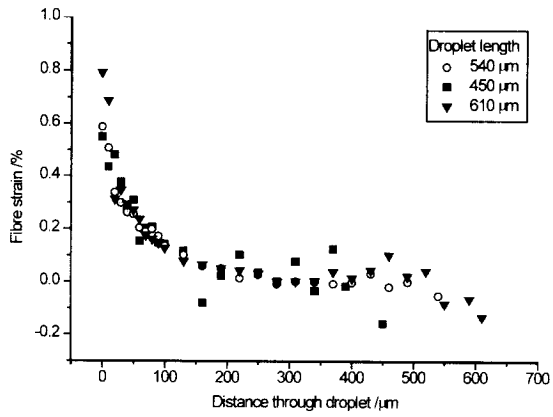

Fig. 11. Strain distribution as a function of droplet length. Knife edge separation 80 μm.

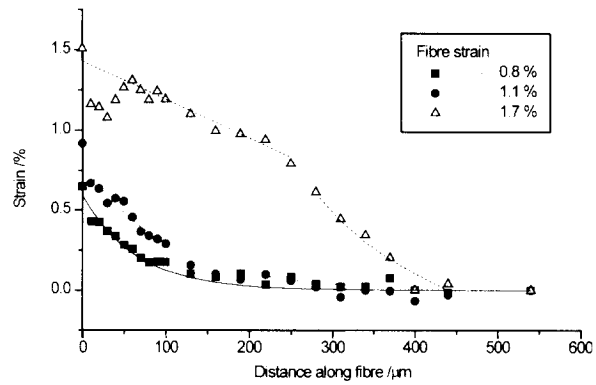

Fig. 12. Strain distribution in a droplet of 440 μm in length with knife edge separation of 50 μm as a function of strain in loaded part of fibre. The solid lines are fits to the theory described in the text.

very much like those observed in the previous figures. Indeed the lines shown on Fig. 12 for the two curves at lower strain were drawn using equation 2 with the same value of n as used for the data of Fig. 7 restrained at 50 μm knife edge gap. With higher levels of strain in the loaded part of the fibre it can be seen that the form of the strain distribution changes significantly. There is a region where the strain decreases linearly followed by a region in which there is shear lag type behaviour. The data are of the form expected where there is partial debonding of the interface. The debonding takes place over the initial portion of the embedded fibre, up to 250 μm, this is then followed by elastic stress transfer. Previous work on the pull-out test[42] has shown that the strain in the debonded part of the fibre can be found from the balance of forces argument which gives rise to the expression[41]

$$\varepsilon_f = \frac{2\tau_i(i-x)}{rE_f} \tag{5}$$

where τ_i is the frictional shear stress, i is the point where a line fitted to the data in the debonded region intercepts the distance axis and the other symbols are as defined previously. The strain in the elastic part of the droplet can be given by modifying eqn (2) to use the bonded, rather than total, length of the fibre. In Fig. 13 the curve at the highest load level was fitted using these equations assuming that the frictional shear stress is 10·5 MPa and that n is 0·07. It can be seen from the figure that these equations fit the data reasonably well. It is interesting to note that the value of n is the same as that required to fit the data of Fig. 7 for a knife edge gap of 80 μm, i.e. at a separation where the finite element analysis shows that there is little effect of the knife edges upon the shear stress distribution. Thus the strain data recorded for this test can be explained and fitted using the existing theory for the pull-out test. The value of the frictional shear stress obtained for this system is exactly the same as the average value obtained by Bannister *et al.*[42] from pull-out tests on high modulus Twaron fibres in a similar resin. The shear yield stress of

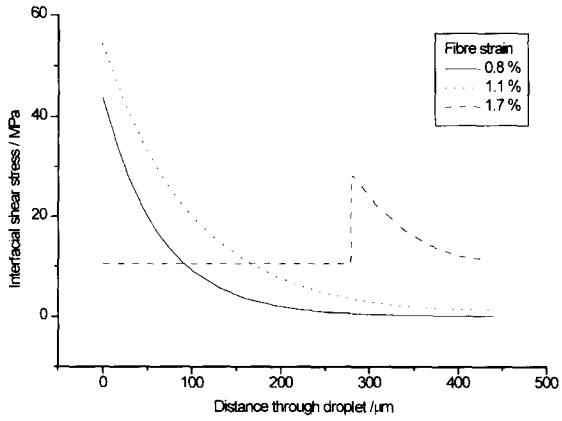

Fig. 13. Interfacial shear stress distributions calculated from the data of Fig. 12 using the theory outlined in the text.

this resin was found to be 43 MPa.[42] The interfacial shear stress data calculated at a fibre strain of 0·8% and shown in Fig. 13 are consistent with this as are the data for a sample with 1·7% fibre strain. The data obtained for the sample under a fibre strain of 1·1% lead to shear stresses close to the fibre end which are apparently greater than the shear yield stress for the matrix. This is probably caused by the fitting to the low number of data points and the comparatively high random error in them caused by the difficulty in performing the measurements.

4 CONCLUSIONS

It was clearly shown that by use of Raman spectroscopy the strain distribution in an embedded fibre during microbond tests can be measured. This has shed some light on the interfacial shear stress distribution in the embedded fibre. In contrast to the assumption normally made in the analysis of data from this micromechanical test the interfacial shear stress is not constant. At low applied loads the strain and shear stress distributions are much as would be expected from shear lag theory. At higher loads this is no longer true. In the example presented in this paper, in Fig. 13, evidence of debonding can be observed. It can also be seen from the experimental data presented in Figs 7 and 8, the finite element analysis of Fig. 10 and the values of n required to fit the data to theory that the position of the grips which support the microdroplet is important and directly affects the interfacial shear stress distribution and its maximum value. The finite element analysis shows that once the knife edges are placed a few fibre diameters away from the fibre, the stress distribution becomes insensitive to their position. If the knife edges are placed close to the fibre then the strain and stress distributions and in particular the maximum interfacial shear stress is very dependent upon gripping position. This is contradictory to the recommendations of Chou *et al.*[43] who suggest that the knife edges should be placed close to the fibre. The data from the conventionally performed and analysed microbond test shows that the values derived for the average interfacial shear stress are much lower than the actual maximum shear stresses. The values obtained for the conventional test were not very dependent upon the position of the knife edge supports, even though the Raman data shows this to be a critical factor controlling the shear stress distribution and maximum interfacial shear stress. It is clear from these observations that a method of data reduction which assumes that the interfacial shear stress is constant under all loading conditions is not appropriate. In none of the cases examined was the interfacial shear stress constant. In addition, interfacial failure will not occur because of the presence of some average level of interfacial shear stress but because of the maximum interfacial shear stress being high enough to cause, for example, rupture of the interface or yielding of the matrix close to the interface. In fact it is now clear that the failure occurs in two stages as seen in Figs 12 and 13. The strains and interfacial shear stresses increase, but the shape of the distribution remains the same as the external load is increased. Failure is then initiated, in this case by a debonding process, and this propagates along the fibre. The maximum interfacial shear stress is the stress at the point where the fibre enters the droplet just before the interface begins to fail. In the conventionally performed test the failure force is recorded. At this point the force consists of that which is required to increase the shear stress to its maximum plus the force necessary to propagate the failure along the interface. There are thus at least two sources of variation in the data presented in Figs 3–5. One is variation caused by the effect of the position of the knife edges. If the droplet is not central between these then the stress concentration effect may vary from sample to sample. The second effect comes from the variation in the frictional strength of the interface from sample to sample as demonstrated for the similar pull-out test by Bannister *et al.*[42]

It is now necessary to redefine the procedures used to gather the experimental data and for the calculation of interfacial shear stresses in the light of the observations presented here and elsewhere.[42,44] The shear lag type models do fit the strain distributions, but the force required to calculate the interfacial shear strength is not the failure load of the specimen. The force required is that at which the sample starts to fail. At this point the strain and interfacial shear stresses fit the shear lag type distributions and the maximum interfacial shear stress is reached, as noted earlier. In principle this can be obtained from careful analysis of the load–displacement curve since the compliance of the sample will change slightly at this point. This change in slope is not easy to detect and some recommendations for a technique which would allow this approach to be used have been made by one of the authors elsewhere.[44] In essence, the suggested method is to use not one but two droplets.

One of these would be restrained, the other displaced. The load–displacement curve would be recorded and the change in stiffness of the sample would indicate the load at which yielding or debonding occurred. This load could then be used to calculate the interfacial shear strength using a shear lag model. A similar suggestion was made by Hampe and Marotzke.[45]

ACKNOWLEDGEMENT

The finite element modelling was undertaken using the LUSAS finite element modelling software supplied by FEA Ltd.

REFERENCES

1. Kelly, A. and Tyson, W. R., *J. Mech. Phys. Solids*, 1965, **13**, 329.
2. Chua, P. S. and Piggott, M. R., *Compos. Sci. Technol.*, 1985, **22**, 33.
3. Favre, J. P. and Merienne, M. C., *Int. J. Adhesion Adhesives*, 1981, **1**, 311.
4. Desarmot, G. and Favre, J.-P., *Compos. Sci. Technol.*, 1991, **42**, 151.
5. Penn, L. S. and Lee, S. M., *Fibre Sci. Tech.*, 1982, **17**, 91.
6. Marshall, P. and Price, J., *Composites*, 1991, **22**(1), 53.
7. Broutman, L. J., *Polym. Eng. Sci.*, 1966, **6**, 263.
8. Pitkethly, M. J. and Doble, J. B., *Compos.*, 1990, **21**(5), 389.
9. Frazer, W. A., Ancker, F. H. and DiBennedetto, A. T., *Proceedings of the 30th Conference on Reinforced Plastics*. SPI section 22A, 1975.
10. Broutman, L. J., Interfaces in Compos., ASTM STP 452, pp. 27–41, 1969.
11. Drzal, L. T., Rich, M. J. and Lloyd, P. F., *J. Adhesion*, 1983, **16**, 133.
12. Gaur, U. and Miller, B., *Compos. Sci. Technol.*, 1989, **34**, 35.
13. Miller, B., Muri, P. and Rebenfeld, L., *Compos. Sci. Technol.*, 1987, **28**, 17.
14. Pitkethly, M. J., Favre, J.-P., Gaur, U., Jakubowski, J., Mudrich, S. F., Caldwell, D. L., Drzal, L. T., Nardin, M., Wagner, H. D., Di Landro, L., Hampe, A., Aristead, J. P., Desaeger, M. and Verpoest, I., *Compos. Sci. Technol.*, 1993, **48**, 205.
15. Wagner, H. D., Gallis, H. E. and Wiesel, E., *J. Mater. Sci.*, 1993, **28**, 2238.
16. Banbaji, J., *Compos. Sci. Technol.*, 1988, **32**, 183.
17. Piggott, M. R., *Load Bearing Fibre Composites*. Pergamon Press, Oxford, UK, 1980, p.83.
18. Day, R. J., *Deformation and Fracture of Composites*. Institute of Materials, 1993.
19. Marotzke, C., *Interfacial Phenomena in Compos. Materials '91*, ed. I. Verpoest and F.R. Jones. Butterworths, 1991, p.69.
20. Young, R. J. and Day, R. J. In: *Integration of Fundamental Polymer Sci. Technol.–5*, ed. P. J. Lemstra and L. A. Kleintjens. Elsevier Applied Science London, in press.
21. Young, R. J., Lu, D. and Day, R., *J. Polymer International*, 1991, **24**, 71.
22. Yang, X., Hu, X., Day, R. J. and Young, R. J., *J. Mater. Sci.*, 1992, **27**, 1409.
23. Young, R. J., Day, R. J., Ang P. P., Stanford, J. L. and Hu, X., *Proceedings of the 1st International Conference on Deformation and Fracture of Composites*, The Plastics and Rubber Institute, Manchester, **19**, 1991.
24. Day, R. J. and Marquez, M., In *Interfacial Phenomena in Composite Materials '91*, ed. I. Verpoest and F.R. Jones. Butterworth–Heinemann Ltd, Oxford, 1991, pp. 65–68.
25. Galiotis, C., Robinson, I. M., Young, R. J., Smith, B. J. E. and Batchelder, D. N., *Polym. Commun.*, 1985, **26**, 354.
26. Young, R. J. and Day, R. J., *Br. Polym. J.*, 1989, **21**, 17.
27. Day, R. J. and Marquez, M., In *Interfacial Phenomena in Compos. Materials '91*, ed. I. Verpoest and F.R. Jones. Butterworth–Heinemann Ltd, Oxford, 1991, pp. 65–68.
28. Andrews, M. C., Day, R. J., Hu, X. and Young, R. J., *J. Mater. Sci. Lett.*, 1992, **11**, 1344.
29. Gu, X. H., Day, R. J. and Young, R. J., *Proceedings of the 2nd International Conference on Deformation and Fracture of Composites*, 1993.
30. Day, R. J., *Proceedings of the 2nd International Conference on Deformation and Fracture of Composites*, 1993.
31. Andrews, M. C., Young, R. J. and Day, R. J., *Proceedings of the Sixth European Conference on Composite Materials*, Woodhead Publishing Ltd, 1993, p. 133.
32. Andrews, M. C., Day, R. J., Hu, X. and Young, R., *J. Compos. Sci. Technol.*, 1993, **48**, 255.
33. Andrews, M. C., Young, R. J. and Day, R. J., In *Developments in the Science and Technol. of Compos. Materials*, ed. A. R. Bunsell, A. Kelly and A. Massiah. Woodhead Publishing Ltd, Cambridge, 1993, p133.
34. Andrews, M. C., Day, R. J., Patrikis, A. K. and Young, R., *J. Composites*, 1994, **25**, 745.
35. Penn, L. S. and Milanovich, F., *Polymer*, 1979, **20**, 31.
36. Edwards, H. G. M. and Hakiki, S., *Br. Polym. J.*, 1989, **21**, 505.
37. Kawabata, S., *J. Textile Institute*, 1990, **81**(4), 432.
38. Baltussen, J. J. M. and Northolt, M. G., *J. Rheology*, 1997, **41**(3), 575.
39. Cox, H. L., *J. App. Phys.*, 1952, **3**, 72.
40. Takau, A. and Arridge, R. G. C., *J. Phys. D: Appl. Phys.*, 1973, **6**, 2038.
41. Kelly, A. and McMillan, N. H., *Strong Solids*. Oxford Science Publications, 1986.
42. Bannister, D. J., Ph.D thesis, UMIST, 1996.
43. Chou, C. T., Gaur, U. and Miller, B., *Compos. Sci. Technol.*, 1994, **51**(1), 111.
44. Day, R. J., Interfaces in Carbon and polymeric fibre composites. In *Proceedings of workshop held February 1–2 1995, Kaiserslauten*, ed. H.-J. Jacobasch, pp.116–126.
45. Hampe, A. and Marotzke, C., *J. Reinf. Plast. Compos.*, 1997, **16**(4), 341.